



Microstructure and high temperature transport properties of high quality epitaxial SrFeO_{3-δ} films

C. Solís^a, M.D. Rossell^b, G. Garcia^c, A. Figueras^a, G. Van Tendeloo^b, J. Santiso^{a,*}

^a Centro de Investigación en Nanociencia y Nanotecnología, CIN2/CSIC, Campus UAB, 08193 Bellaterra, Spain

^b Electron Microscopy for Materials Research (EMAT), University of Antwerp, Groenenborgerlaan 171, B-2020 Antwerpen, Belgium

^c Grup de Nanomaterials i Microsistemes, UFMI, Departament de Física, UAB, 08193 Bellaterra, Spain

ARTICLE INFO

Article history:

Received 4 February 2008

Received in revised form 3 April 2008

Accepted 2 June 2008

Keywords:

Thin films

Microstructure

Conductivity

Oxygen sensors

ABSTRACT

We report the high temperature electronic transport properties of SrFeO_{3-δ} epitaxial thin films obtained by pulsed laser deposition on NdGaO₃(110) substrates. The films show total conductivity higher than the bulk material and apparent activation energy of about 0.12 eV in O₂, lower than reported values for SrFeO_{3-δ} films. The conductivity dependence with oxygen partial pressure shows a power dependence with an exponent close to +1/4, in agreement with expected point defect equilibrium. For a given oxygen partial pressure, the temperature coefficient of resistance (TCR) shows a low positive value of about 1.5–2.5 10⁻³ K⁻¹, which is still suitable for resistive oxygen sensing applications. The transport properties of the films are discussed in view of their particular microstructure.

© 2008 Elsevier B.V. All rights reserved.

1. Introduction

Perovskite-type oxides exhibiting high electronic conductivity at elevated temperatures are interesting for their potential applications, such as high-temperature solid oxide fuel cells, or gas sensing materials. In the case of gas sensors, they represent an alternative for resistive-type sensors based on SnO₂, TiO₂ and CeO₂-ZrO₂ semiconducting oxides [1–3]. SrFeO_{3-δ} perovskite oxide has received special attention as potential candidate for oxygen sensors in direct fuel injection engines due to its strong sensitivity to oxygen partial pressure variations and negligible cross-sensitivity to temperature fluctuations [4–7]. Besides, the study of the SrFeO_x (2.5 < x < 3) system is also important from a fundamental point of view since a clear correlation between the oxygen vacancies ordering and its sensing properties has been already pointed out [8]. Although thin films are expected to have a faster response, most of the sensing studies in SrFeO_{3-δ} have been performed in bulk samples [9–11]. However, non-stoichiometric SrFeO_{3-δ} films have been prepared by different techniques: polycrystalline thin films by sol gel [12,13] and citrate method [14]; while highly crystalline films have been prepared by pulsed laser deposition (PLD) [3–5,15–19]. The films showed a large oxygen sensitivity at high temperature, particularly in the low oxygen pressure range ($p_{O_2} \sim 10^{-4}$ atm) where there was observed a phase

transformation from cubic perovskite to brownmillerite structure [5]. High temperature gas sensors based on SrFeO_{2.5+x} material have been already fabricated onto microhotplates and successful chemical sensor functionality has been demonstrated [20]. More recently severely reduced SrFeO₂ ceramics have shown infinite-layer structure with very promising ionic conductivity at lower temperatures [21].

In the present work, we report a complete study of film microstructure and high temperature conductivity properties, under different atmospheres, of high quality epitaxial SrFeO_{3-δ} thin films obtained by PLD.

2. Experimental

A dense ceramic pellet of pure SrFeO_{3-δ} (SFO) compound was prepared by a solid-state reaction from a stoichiometric (Sr:Fe=1:1) mixture of SrCO₃ and Fe₂O₃ sintered in air at 1000 °C in order to be used as target for the PLD experiment. X-ray diffraction (XRD) of the sintered targets confirmed the complete formation of the cubic phase, in good accordance with the reported results [22]. SrFeO_{3-δ} films were deposited by using a Nd:YAG pulsed laser with tripled frequency (355 nm wavelength), 9 ns pulse length, 10 Hz repetition rate, and 2–3 J/cm² energy density per pulse. Different number of pulses was used in order to grow films from 37 nm to 240 nm. The films were deposited on NdGaO₃ (110) (NGO) single crystal substrates at oxygen pressures of 1×10^{-2} mbar, and substrate temperatures of 750 °C. The NdGaO₃ substrate has a perovskite structure with orthorhombic lattice parameters $a=0.54333$ nm, $b=0.55036$ nm, and $c=0.77157$ nm [23]. Therefore its (110) plane cut exhibits a pseudocubic lattice with

* Corresponding author. Research Centre for Nanoscience and Nanotechnology, CIN2 (CSIC-ICN), Campus UAB, 08193 Bellaterra, Barcelona, Spain. Tel.: +34 935814700; fax: +34 935813717.

E-mail address: jose.santiso@cin2.es (J. Santiso).

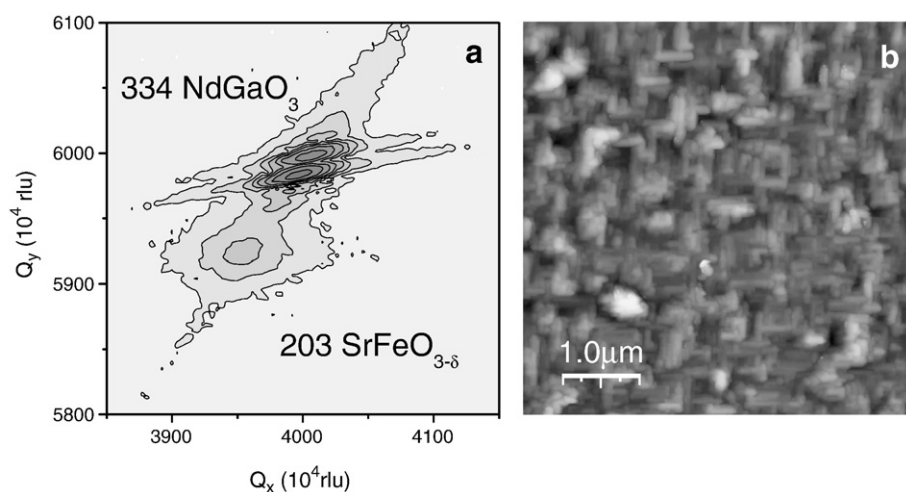


Fig. 1. (Color online) (a) XRD Reciprocal space map of the 203 reflection for a 240 nm thick $\text{SrFeO}_{3-\delta}$ film along with the 334 reflection of the NGO substrate (equivalent to a 203 reflection of a pseudocubic primitive cell). (b) AFM image of a film showing the presence of rectangular grains on the surface.

in-plane lattice parameters 0.3863 nm and 0.3854 nm. Taking as a reference the reported cell parameter of 0.3864 nm for cubic $\text{SrFeO}_{2.875}$ [22], the lattice mismatch expected for epitaxial films is 0.02% and -0.26% along each perpendicular direction. The thickness of the films was determined by XRD reflectometry for the thinner films and the growth rate extracted from this data was used to estimate the thickness of the thicker layers. Wavelength dispersive spectrometry (WDS) was used to estimate the cation concentration in the films by applying the STRATA software. The structure of the films was studied by XRD using an Advanced D8 Bruker diffractometer with a four angle goniometer and GADDS detector. The microstructure of the films was analyzed by transmission electron microscopy (TEM) using a JEOL 4000EX microscope operated at 400 kV. Cross-section samples were cut parallel to a cube plane of the NGO substrate and mechanically ground to a thickness of about 20 nm, followed by final ion-milling under grazing incidence until electron transparency was obtained. Image simulations were made with the MacTempas software. The conductivity of the films was determined by AC impedance measurements in the frequency range 5 Hz–13 MHz using an HP 4192A impedance analyser. Two parallel stripe-shaped electrodes were painted on the surface of each sample with Ag paste.

3. Results and discussion

The deposited films presented an epitaxial growth onto the substrates with their c -axis in the direction perpendicular to the films plane. The average out-of-plane c and the in-plane a parameters, for each film, was calculated from the angular position of the 203 reflection determined from reciprocal space maps as shown in Fig. 1.a. The lattice parameters obtained from these reciprocal space maps were 0.3904 nm for the out-of-plane parameter and 0.3899 nm for the in-plane parameter. Similar values were obtained for films with different thickness. The slight difference between in-plane and out-of-plane parameter is within the accuracy of the measurement and should not be attributed to any tetragonal deformation induced by oxygen vacancy ordering in the film, for which we did not find any evidence. Therefore, the film structure should be considered as cubic in the as-deposited samples. However, cell parameters are larger than the value 0.3851 nm reported for cubic SrFeO_3 bulk samples [22]. No variations in the cell parameter were observed after subsequent annealing in O_2 atmosphere. The observed cell expansion could not be attributed to any in-plane strain induced by the substrate, because no coherent growth with the substrate was observed. Given that the equilibrium cell parameters, and so the cell volume, are expected to

increase when reducing the oxygen composition as reported in previous studies performed on ceramic samples [22], we might consider that our films present under-stoichiometric oxygen composition. A rough estimate of the cell volume in our films, assuming that the in-plane parameter is the same in both substrate directions, is about 0.059 nm^3 , half way between 0.057 and 0.061 nm^3 reported for fully oxidized cubic SrFeO_3 and brownmillerite $\text{SrFeO}_{2.5}$, respectively [16], and still above the 0.058 nm^3 reported for $\text{SrFeO}_{2.75}$ brownmillerite [22]. This would correspond to an oxygen content of $2.5 < x < 2.75$

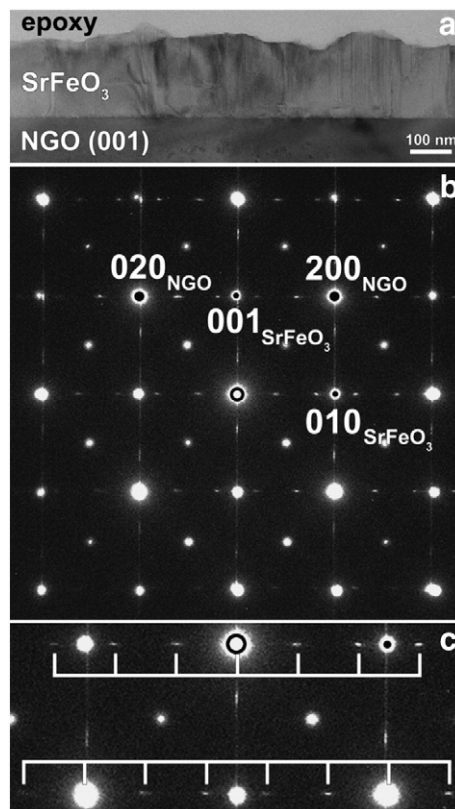


Fig. 2. (a) Cross-section low magnification image of a $\text{SrFeO}_{3-\delta}$ film along a cube direction and (b) the corresponding ED pattern. (c) Enlarged part of (b) showing the presence of diffuse streaks along [001] and [010] of the SrFeO_3 film. The white brackets outline the streaking maxima along [010].

in the films. Unfortunately, it is very difficult to determine the oxygen composition of our layers with the conventional techniques and in a reliable manner due to their reduced thickness as well as to the presence of oxygen also in the substrate. The Sr:Fe ratio measured by WDS was 1.00:0.97. This might indicate a slight deviation from stoichiometry, although it is still within the accuracy of the measurement. By using the AFM technique we were able to characterize the surface morphology. The samples were rather smooth but, as it can be seen in Fig. 1.b. The surface was mainly formed by rectangular crystals of a maximum length of 400 nm, less than 100 nm wide and 20 nm high, approximately. Since no other phases were detected by the XRD, we assumed the needle shaped surface corresponds to the SFO perovskite material.

Cross-section specimens were then prepared in order to assess the origin of such surface morphology. A cross-section low magnification image and the corresponding electron diffraction (ED) pattern are shown in Fig. 2.a and b, respectively. Cross-section TEM shows that the SrFeO₃ films are not uniform but present protuberances that correspond to the mutually perpendicular needles detected by AFM. These bulges arise from microstructural defects in the films, as will be shown below. The ED is a superposition of the patterns from substrate and film (Fig. 2.b). These reflections form a square pattern. The following epitaxial relation is found: (110)NGO(001)SrFeO₃, [11 0] NGO [010]SrFeO₃, in accordance with the XRD results. A detailed examination of the ED pattern (Fig. 2 c) indicates the presence of diffuse streaks along the cube directions of the SrFeO₃ film. These

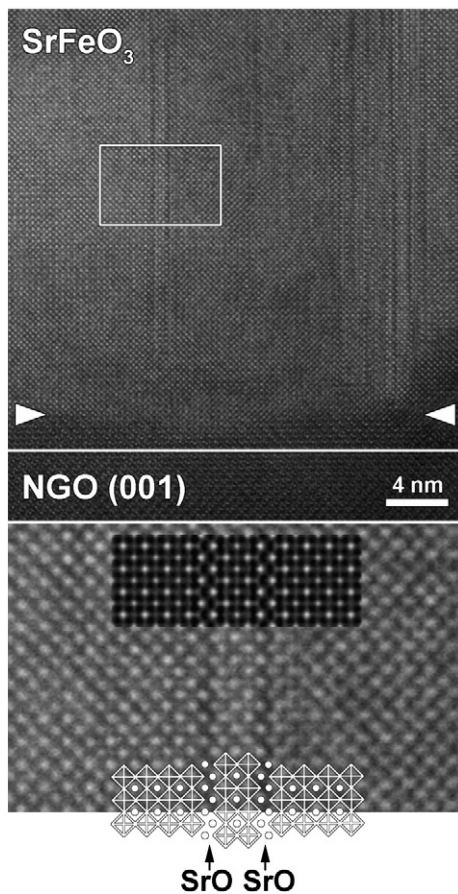


Fig. 3. Top: Cross-section HREM image of the SrFeO₃/NGO(110) interface (indicated by white arrowheads). Note the presence of vertical (010) planar defects with different contrast. Bottom: Enlarged area showing (010) planar defects due to the insertion of extra SrO rock salt-type layers in the SrFeO₃ structure. A polyhedra arrangement and a calculated image, for a defocus value $\Delta f = -67.5$ nm and a thickness $t = 7.5$ nm, are shown as insets. From a comparison of the simulated image with the experimental image, bright dots correspond to columns of heavy atoms.

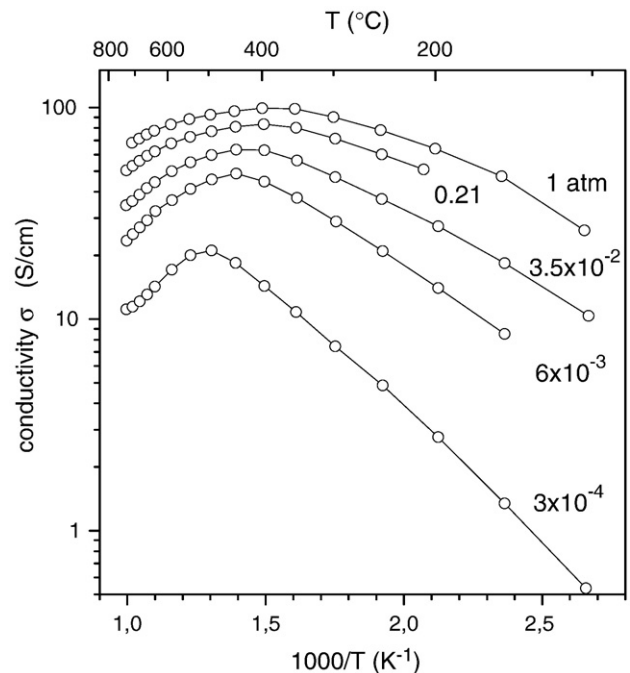


Fig. 4. Conductivity dependence with temperature of a 67 nm thick SFO film at different oxygen partial pressures.

reflections do not correspond to the SrFeO₃ but are related to the presence of planar defects both parallel and perpendicular to the substrate surface, visible in the low magnification cross-section image (Fig. 2a). Moreover, the streaking along the [010]SrFeO₃ axis shows a series of maxima (outlined by white brackets in Fig. 2.c) with a long parameter $\sim 5 \cdot a_{\text{SFO}} \approx 1.96$ nm. A cross-section HREM image of the SrFeO₃/NGO(110) interface is shown in Fig. 3. In this image only vertical (010) planar defects are observed, corresponding to the areas with different contrast. This type of defects is often associated with a large amount of dislocations detected at the substrate-film interface (marked with white arrowheads in Fig. 3, top). The planar defects are due to the insertion of an extra SrO rock salt-type layer in the SrFeO₃ structure resulting in a shift over $a_{\text{SFO}}/2$ between adjacent layers along a direction parallel to the SrO layer, as shown by the coordination polyhedra arrangement in Fig. 3 (bottom). Additional SrO rock salt-type layers inserted every two perovskite-type layers can explain the intense maxima at $\sim 5 \cdot a_{\text{SFO}}$ found in the streaking lines of the ED patterns (Fig. 2.c). The formation of these Sr-enriched regions could be consistent with the slight deviation from Sr:Fe stoichiometry measured by WDS. These extra SrO planes might also contribute to the larger measured cell parameters of the SrFeO_{3- δ} films, and could be responsible for the cell volume variation rather than only due to oxygen composition variations.

Transport measurements were carried out using AC impedance spectroscopy to differentiate possible contributions to the overall resistance from the grains, grain boundaries, and other macroscopic features, as often observed in polycrystalline ceramics. In planar measurement on thin films the capacitance associated to the material and grain boundaries scales directly with the thickness of the sample, whereas the resistance does it inversely. For a film thickness below 100 nm the capacitance associated to the film is not expected to reach the pF range, much lower than the stray capacitances of the measuring setup of about 10 pF. In our samples the complex impedance spectra shows always single arcs corresponding to the film resistance along with the stray capacitance. After heating the furnace to 800 °C and filling it with a slow flux of different mixture gases (from 1 atm O₂ to 10⁻⁴ atm), the measurements were taken at 50 °C intervals on cooling down under the same atmosphere, with 25 min stabilizing period at each temperature. In Fig. 4 we show the

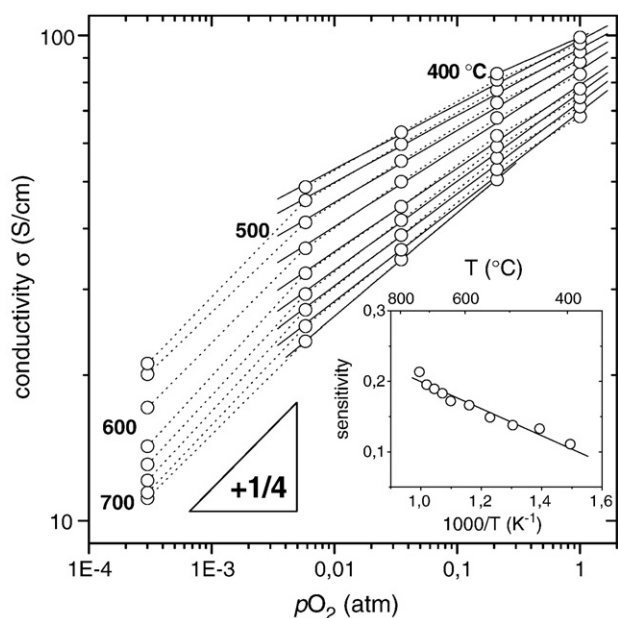


Fig. 5. Conductivity behaviour of a 67 nm thin films as a function of pO_2 at different temperatures. The inset shows the film sensitivity to pO_2 changes (slope of the conductivity curves) as a function of temperature.

Arrhenius representation of the conductivity of a 67 nm thick film as a function of temperature for different oxygen partial pressures. Below 400 °C, the conductivities show a thermal activated behaviour with activation energies E_a ranging from 0.12 eV at 1 atm to 0.24 eV at $3 \cdot 10^{-4}$ atm. This is consistent with the small-polaron hopping mechanism found for the bulk samples [9], although the measured E_a values are smaller than those reported for SrFeO_{2.5+x} films between 0.2 and 0.5 eV [5]. Above this temperature the conductivity decreases because the film starts losing oxygen. No any anomalies in the slope of the curve were observed in the temperature range around 300 °C which could be an indication that no oxygen order-disorder transition takes place in the films as it was previously reported by other authors on oxygen deficient films deposited by PLD [5,24]. We can also observe that the conductivity decreases upon lowering the pO_2 , as corresponds to p -type conductivity. At 750 °C, in pure O₂ ($pO_2 = 1$ atm), the conductivity of the films was 70 S/cm largely above that of ceramic samples (12 ± 3 S/cm) [6,10,11]. This improvement in the transport properties should be related to the particular microstructure of the epitaxial films. It is very likely that the presence of a high density of planar defects such as those observed in the films might define higher mobility paths for the diffusion of charge carriers lowering the apparent activation energy and thus increasing the attained conductivity values. At room temperature (and in 1 atm O₂) the film conductivity was about 14.3 S cm^{-1} (resistivity of 0.07 Ω-cm) that is in accordance with reported resistivity values of 0.04 Ω-cm on epitaxial SFO/SrTiO₃ films [16]. In the high temperature range above 400 °C the conductivity values in Fig. 4 reflect the equilibrium attained for each corresponding pO_2 after oxygen exchange with the gas atmosphere. These values are depicted in Fig. 5 as a function of pO_2 (in a log-log plot). In the measured temperature range and $pO_2 > 10^{-4}$ atm, SrFeO_{3-δ} films exhibit the expected p -type conductivity in which the electrical conductivity (σ) follows a $\sigma \propto p(O_2)^{+1/4}$ dependence consistent with the full compensation of oxygen donors by iron acceptors [9–11]. The higher the temperature the closer to the +1/4 dependence, while for lower temperatures the slope of the curve is progressively smaller, particularly in the high pressure range $pO_2 > 10^{-2}$ atm. This might

be related to a partial compensation of the iron acceptors, somehow affected by the presence of the extended planar defects observed in the film microstructure. This is evidenced by the increase of the slope with temperature, which corresponds to the sensitivity to pO_2 variations shown in the inset. Another significant observation is the low temperature dependence of the conductivity for a fixed pO_2 (changes in $\sigma < 20\%$ for a temperature span $\Delta T \sim 100$ °C from 650 °C to 750 °C, in the whole pO_2 analysed). This corresponds to a TCR, i.e.: temperature coefficient of resistance $(\Delta R/R)/\Delta T$, of about $1.5\text{--}2.5 \cdot 10^{-3} \text{ K}^{-1}$, very close to the value of about 10^{-4} K^{-1} reported necessary for temperature independent sensors [24].

In summary, we have shown that film microstructure might have an important influence in the transport properties of SrFeO_{3-δ} thin films in view of their application for resistive oxygen gas sensing devices. Particularly, slight deviations from the Sr:Fe composition might induce the presence of planar defects which could be beneficial for enhancing carrier mobilities. Although these are very promising results further improvement is still necessary in order to ascertain the role of the cation composition, for instance by using off-stoichiometric PLD targets for thin film deposition. Besides, for practical applications, additional issues, such as sensitivity in the presence of other gases, long term chemical stability, as well as kinetic response, should be addressed, and will be the subject of a further study.

Acknowledgements

This research was partially supported by the MAT2005-02601 project from the Spanish Government. The TEM/HREM work has been performed within the framework of IAP V-1 of the Belgian government and the GBOU contract of the Flemish government.

References

- [1] G. Sberveglieri, Sens. Actuators B 23 (1995) 105.
- [2] A. Rothschild, H.L. Tuller, J. Electroceram. 17 (2006) 1005.
- [3] J.W. Fergus, Sens. Actuators B 123 (2007) 1169.
- [4] M.L. Post, J.J. Tunney, Sens. Actuators B 59 (1999) 190.
- [5] J. Tunney, M.L. Post, J. Electroceram. 5 (2000) 63.
- [6] M.L. Post, W. Brian, S.P. Kennepohl, Sens. Actuators B 13–14 (1993) 272.
- [7] M. L. Post, Thin film oxygen sensor, Patent number US5397541 (1995).
- [8] J.B. MacChesney, R.C. Sherwood, J.F. Potter, J. Chem. Phys. 43 (1965) 1907.
- [9] F.W. Poulsen, G. Lauvstad, R. Tunold, Solid State Ionics 72 (1994) 47.
- [10] V.L. Kozhevnikov, I.A. Leonidov, M.V. Patrakeev, E.B. Mitberg, K.R. Poeppelmeier, J. Solid State Chem. 158 (2000) 320.
- [11] A. Rothschild, W. Menesklou, H.L. Tuller, E. Ivers-Tiffée, Chem. Mater. 18 (2006) 3651.
- [12] C. Liang, D.A. Yang, J.J. Song, M.X. Xu, Key Eng. Mater. 280–283 (2005) 315.
- [13] A. Majid, J.J. Tunney, M. Post, J. Margeson, J. Sol-Gel. Sci. Technol. 38 (2006) 271.
- [14] C. Liang, D. Yang, Z. Yang, F. Hou, M. Xu, Surf. Coat. Technol. 200 (2005) 2515.
- [15] Z. Wang, T. Sasaki, N. Koshizaki, J.J. Tunney, M.L. Post, Thin Solid Films 437 (2003) 95.
- [16] H. Yamada, M. Kawasaki, Y. Tokura, Appl. Phys. Lett. 80 (2002) 622.
- [17] T. Yu, Y.F. Chen, Z.G. Liu, L. Sun, S.B. Xiong, N.B. Ming, Z.M. Zhou, J. Appl. Phys. A Mater. Sci. Process. 64 (1996) 69.
- [18] O.I. Lebedev, J. Verbeeck, G. van Tendeloo, N. Hayashi, T. Terashima, M. Takano, Phil. Mag. 84 (2004) 3825.
- [19] Y. Wang, J. Chen, X. Wu, Mater. Lett. 49 (2001) 361.
- [20] O. Grudin, R. Marinescu, L.M. Landsberger, M. Kahrizi, G. Frolov, J.D.N. Cheeke, S. Chehab, M. Post, J. Tunney, X. Du, D. Yang, D. Segall, J. Vac. Sci. Technol. A 20 (2002) 1100.
- [21] Y. Tsujimoto, C. Tassel, N. Hayashi, T. Watanabe, H. Kageyama, K. Yoshimura, M. Takano, M. Ceretti, C. Ritter, W. Paulus, Nature 450 (2007) 1062.
- [22] J.P. Hodges, S. Short, J.D. Jorgensen, X. Xiong, B. Dabrowski, S.M. Mini, C.W. Kimball, J. Solid State Chem. 151 (2000) 190.
- [23] W. Marti, P. Fischer, F. Altorfer, H.J. Scheel, M. Tadin, J. Phys. Condens. Matter. 6 (1994) 127.
- [24] R. Moos, W. Menesklou, H.J. Schreiner, K.H. Härdtl, Sens. Actuators B 67 (2000) 178.